Pharmacological Research 219 (2025) 107916

Contents lists available at ScienceDirect

Pharmacological Research

journal homepage: www.elsevier.com/locate/yphrs

Ultrasound-activated poly(butyl cyanoacrylate) microbubbles enhance the therapeutic effect of Doxil

Julia Blöck, Lea Imschweiler, Rahaf Mihyar, Junlin Chen, Roman Barmin, Susanne Koletnik, Roger M. Pallares, Twan Lammers, Anne Rix *, Fabian Kiessling *

Institute for Experimental Molecular Imaging, RWTH Aachen University Hospital, Forckenbeckstraße 55, Aachen 52070, Germany

ARTICLE INFO

Keywords:
Sonopermeation
Ultrasound
PBCA
Microbubbles
Doxil
Tumor

ABSTRACT

Microbubble-assisted ultrasound can improve the delivery of drugs to tumors by temporarily opening biological barriers, a process commonly referred to as sonopermeation. The type of microbubbles plays a key role in this context, with size distribution and the associated degree of polydispersity being important determinants of treatment efficiency, as a broad size distribution makes it difficult to control the induced effects. Poly(butyl cyanoacrylate) (PBCA) microbubbles have been shown to be suitable for sonopermeation applications due to their narrow, tunable size distribution and unique acoustic response profile. In this study, we investigated their potential to improve the anti-tumor efficacy of liposomal nanomedicines. First, we demonstrated that PBCA microbubble-assisted sonopermeation enhances the penetration of cell layers and the cellular uptake of 70 kDa dextran *in vitro*. The extravasation of dextran was also promoted in orthotopic murine breast tumors due to increased vascular and stromal permeability. Importantly, combining our sonopermeation protocol using PBCA microbubbles with low-dose Doxil therapy resulted in improved tumor responses, reflected by an inhibition of tumor growth, enhanced apoptosis and reduced cancer cell proliferation. Thus, this study underlines the therapeutic potential of PBCA microbubble-assisted sonopermeation and paves the way for further translational research.

1. Introduction

Micrometer-sized gas-filled particles, known as microbubbles (MBs), are responsive to ultrasound (US) and thereby mechanically interact with their environment in versatile ways [1,2]. MB and US (MB-US) assisted drug is extensively studied to improve the therapeutic outcome of cancer therapy, enabling the spatially and temporally controlled release of therapeutic agents thereby increasing the accumulation of drugs in the tumor tissue, with the aim of reducing the administered dose to alleviate side effects [3–6]. The applied technique is part of a broader trend towards minimally invasive [3], function-preserving interventions, as addressed in other contexts [7]. This is achieved by opening biological barriers, such as tumor vessels or tumor cell membranes, among others, barriers that might impede the delivery of nanomedicines [8]. The underlying mechanisms have been mainly elucidated in *in vitro* experiments and were found to rely on cellular processes such as the opening of cell-cell contacts, generation of transcellular (tunnels) and membrane pores, and the enhancement of endocytic activity, commonly summarized as sonopermeation and sonoporation, respectively [9–11].

Preclinical studies in different cancer types have reported increase in penetration depth of nanomedicines [12], enhanced anti-tumor effects owing to augmented delivery of chemotherapeutic drugs [13–17] or genes downregulating tumor-specific pathways [18,19] upon MB-US treatment. Subsequently, the safety of MB-US treatment in humans was confirmed [20], and following clinical trials have been focused on improving therapeutic outcomes in cancer patients. For instance, chemotherapy treatment of patients with unresectable pancreatic cancer has been more effective in comparison to a retrospective cohort [21] and has led to enhanced shrinkage of breast tumors [22] after MB-US treatment. The used commercial lipid MBs (SonoVue) were excited at low US intensity (mechanical indices $\leq$ 0.3) to induce either stable cavitation (non-destructive responses) [21] or both stable and inertial cavitation (non-destructive and destructive responses) [22]. Other

* Correspondence to: Institute for Experimental Molecular Imaging, RWTH Aachen University Hospital, Medical Faculty, Forckenbeckstraße 55, Aachen 52070, Germany.

E-mail addresses: arix@ukaachen.de (A. Rix), fkiessling@ukaachen.de (F. Kiessling).

https://doi.org/10.1016/j.phrs.2025.107916
Received 10 June 2025; Received in revised form 30 July 2025; Accepted 14 August 2025
Available online 15 August 2025

studies used higher US intensities (mechanical indices between 0.5 and 0.8) to induce inertial cavitation (destructive responses) of commercial lipid MBs (SonoVue). However, high-intensity MB-US treatment in breast cancer patients receiving neoadjuvant therapy did not improve tumor perfusion or tumor response [23]. Similar results were described in a clinical trial enrolling patients with liver metastases, in which the MB-assisted US treatment did not enhance the anti-tumor effect [24].

Yet, there is no clear consensus on whether non-destructive or destructive MB responses are more beneficial in stimulating biological effects *in vivo*. Researchers have postulated that destructive MB responses lead to unwanted vascular ablation [23], although efficient drug accumulation after inducing vascular breakdown in breast cancer xenografts in mice was reported [23,25]. Others, in turn, concluded that non-destructive MB responses are more beneficial for therapeutic purposes, due to a reduced risk of tissue damage and prolonged interaction times of the responding MBs with the targeted tissue [26].

Besides the US settings, the properties of the MBs (*e.g.* size distribution and response profile) strongly influence the biological effects. In particular, polydispersity, as present in most lipid MB formulations, has been identified as a determinant of effect efficiency [27], among other factors [28,29]. These broadly size-distributed (polydisperse) MBs are characterized by a wide range of resonance frequencies, as these are dependent on the MB diameter and the strongest MB response is observed at the resonance frequency. Although polydispersity ensures compatibility with different transducers for diagnostic purposes, MB formulations with narrow size distributions are preferable for therapeutic applications [23] as they increase safety, robustness and reproducibility of the technique.

The *in vivo* studies mentioned above have used broadly size-distributed MBs in combination with different US settings and US transducers to trigger different MB responses. This variety most likely resulted in the stimulation of different biological effects and may account for the inconsistent results reported.

With this in mind, polymeric MBs were found to be promising for MB-assisted US treatment due to their adjustable size distribution, making them more easily controllable in biological environments. Recently, we characterized the US response of narrow size-distributed commercial poly(butyl cyanoacrylate) MBs (PBCA-MBs) and their ability to induce biological effects *in vitro* compared to commercial lipid MBs (SonoVue). The results demonstrated compression-driven US responses and bursting at acoustic pressures $\geq$ 500 kPa (1 MHz), both of which induced biological effects [30]. Previous studies using PBCA-MBs proved their safe application in small [31–33] and large animal models [34], as well as their ability to permeate the blood-brain barrier [35,36] and peripheral tumors [33,37].

The present study is the first to evaluate the therapeutic potential of sonopermeation with PBCA-MBs. After studying the biological effects *in vitro* (Fig. 1 A), we investigated whether PBCA-MBs-assisted sonopermeation efficiently enhances extravasation into tumor tissue by opening biological barriers (Fig. 1 B) and improves the response of orthotopic murine breast cancer to doxorubicin-loaded liposomes (Doxil) (Fig. 1 C). Here, we show that combining PBCA-MB-mediated sonopermeation with low-dose Doxil therapy significantly improved drug response. These findings demonstrate the clinical potential of PBCA-MBs for sonopermeation-assisted drug delivery and support their further translation to advance cancer therapy.

2. Materials and methods

2.1. In vitro experiments

2.1.1. Cell culture and sample preparation

Human umbilical vein endothelial cells (HUVEC) and 4T1 triple-negative breast cancer cells were purchased from PromoCell (Heidelberg, Germany) and ATCC (LCG Standards, Wesel, Germany), respectively, and cultured under standard conditions (37°C, 5 % CO_2 and humidified atmosphere).

HUVEC were cultured in VascuLife basal medium (LifeLine Cell Technology, Troisdorf, Germany) using passages 3 – 7. For detachment, cells were treated with trypsin (0.25 % in 0.05 % EDTA) for no longer than three minutes and the cell suspension was adjusted to a concentration of 5×10^5/ml. A volume of 70 µl of cell suspension was added to the basolateral surface (Fig. 1 A.1) of cell culture inserts (Falcon cell culture inserts, catalog no. 353096, Corning, Kaiserslautern, Germany) by placing them upside down. The insert membrane was coated overnight prior to seeding with collagen G1 solution (Matrix Bioscience, Mörlenbach, Germany) with an equivalent amount of 10 µg/cm^2 collagen, according to the manufacturer's recommendations [38]. After the addition of the cell suspension, the inserts were kept upside down in the incubator for four hours. Finally, the inserts were inverted and 0.8 ml and 0.35 ml VascuLife medium were added to the basolateral and apical chambers, respectively. The cells were cultured for three days to reach confluence. The medium was replaced twice during this time.

4T1 cells (passages 33 – 38) were cultured in Roswell Park Memorial Institute (RPMI) medium supplemented with 10 % fetal bovine serum (FBS) and 1 % antibiotics (penicillin and streptomycin (P/S)) until reaching approximately 80 % confluence. The cells were detached by trypsinization (0.25 % in 0.05 % EDTA, 3 min) and replated onto the apical surface (Fig. 1 A.2) of poly-D-lysine (0.1 mg/ml) coated cell culture inserts using 70 µl of cell suspension at a concentration of 7×10^5/ml. After cell seeding, 1 ml and 0.5 ml cell culture medium (RPMI + 10 % FBS + 1 % P/S) were added to the basolateral and apical compartments of the cell culture insert, respectively. The cells were incubated for a total of three days to reach confluence. The medium was changed twice during this period.

2.1.2. Focused US set up

A previously established focused US (fUS) setup [30,39,40] was used, consisting of a waveform generator (33612 A, Keysight, Penang, Malaysia), a second waveform generator with an integrated oscilloscope function (SDS 1202X+, Siglent, JR Special Electronics, Helmond, The Netherlands), which was coupled to a radiofrequency broadband amplifier (AG 1021 LF, T&C Power Conversion, Inc., New York, USA). A custom-made matchbox was used to amplify the electrical excitation signal and to connect the single-element fUS transducer (V314-SU-F1.00in-PTF, Evident Europe GmbH, Hamburg, Germany, 1 MHz center frequency, 25 mm focal length) to the amplifier. A water tank filled with Milli Q water was used to sonicate samples in a lumox well plate (lumox multiwell, Sarstedt AG & Co. KG, Nümbrecht, Germany) with the fUS transducer mounted vertically from below and the bottom of the lumox well plate immersed in the water. The distance to the transducer was adjusted to its focal length of 25 mm to align the sample with the focal point.

2.1.3. MB-fUS treatment of HUVEC and 4T1 cells

HUVEC or 4T1 monolayers on cell culture inserts were exposed to MB-assisted fUS treatment (MB-fUS) to induce sonoporation or sonopermeation effects (Fig. 1 A-A.2). Sonoporation was evaluated based on cellular uptake of 70 kDa dextran, whereas sonopermeation was assessed by transendothelial/-epithelial electrical resistance (TEER) measurements and diffusion of 70 kDa dextran across the cell monolayers (Fig. 1 A.3). A sample size of n = 3 was scheduled for each cell line and for each readout method. Control samples were sham-treated by handling-only and carried along in the same number.

The previously described fUS setup was used to generate a 10-cycle sine wave at 1 MHz with a pulse repetition of 2 kHz, which was applied for 2 s. The setup was previously calibrated using a 1 mm needle hydrophone (Precision Acoustics, Dorchester, UK) placed inside the lumox well plate [39] to obtain an *in situ* peak negative pressure (PNP) of 600 kPa. Our previous results on PBCA-MBs ultrasound responses showed MB bursting at PNP $\geq$ 500 kPa, which induced significant biological effects [30]. Here, we selected a PNP slightly higher than 500 kPa to

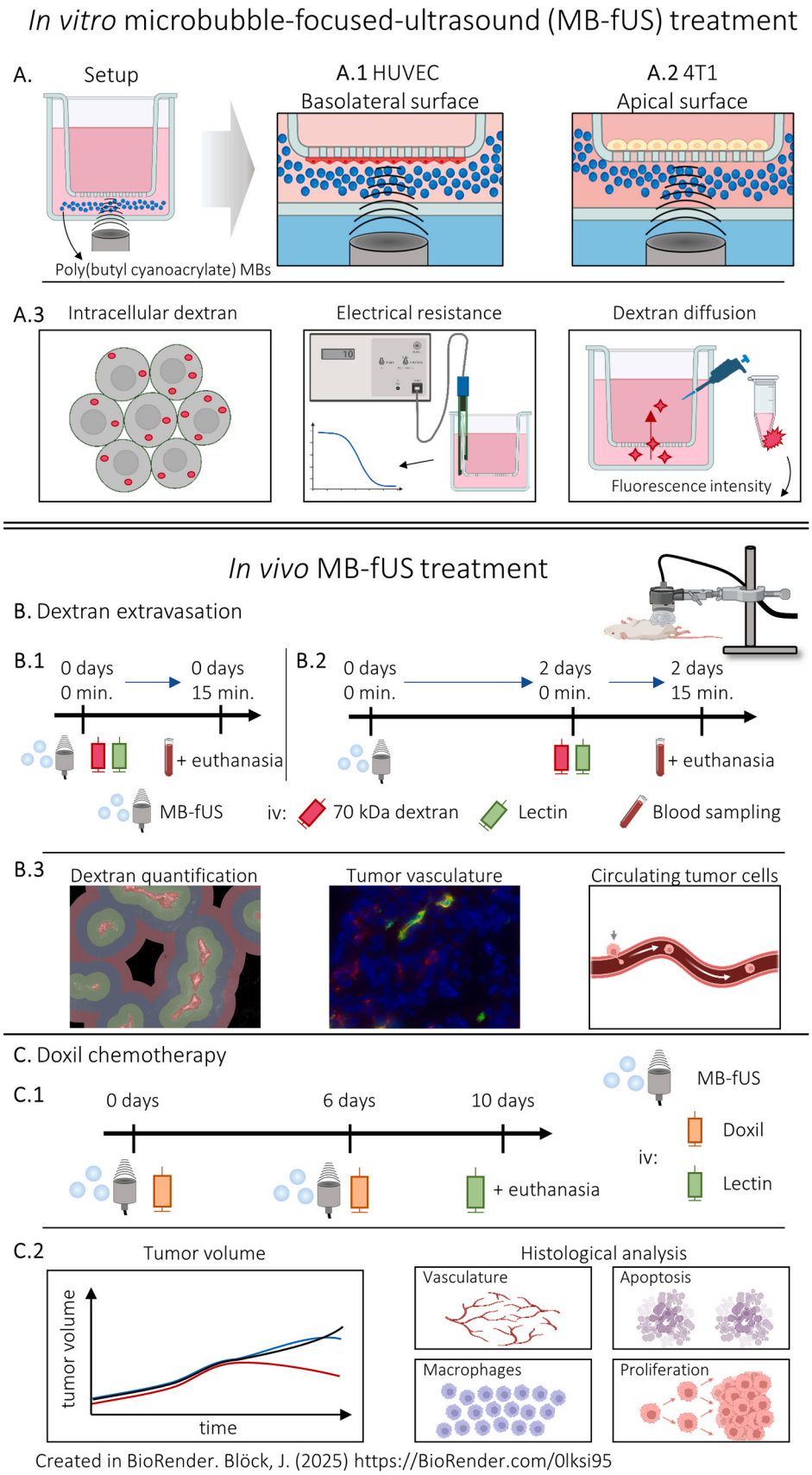

Fig. 1. HUVEC and 4T1 monolayers were treated with microbubble-focused-ultrasound (MB-fUS) using poly(butyl cyanoacrylate) (PBCA) MBs to induce sonoporation and sonopermeation effects (A.1-A.3). PBCA-MB-fUS was applied to murine tumors, to enhance the extravasation of dextran (B.1-B.3) and assess the impact on a low-dose Doxil therapy (C.1 +C.2).

compensate for tissue attenuation during the intended *in vivo* application. With a driving frequency of 1 MHz, this gives a mechanical index of 0.6, which is still far below the clinical threshold of 1.9.

Sonoporation experiments were performed in 300 µl of cell culture medium containing Rhodamine B-labeled 70 kDa dextran (0.25 mg/ml in PBS), wheat germ agglutinin (WGA, Alexa Fluor 488, 5 µg/ml), and Hoechst 33342 solution (1 µg/ml). Dextran was used to detect sonoporation, while WGA and Hoechst were used to stain the cell membranes and nuclei, respectively. Next to that, 2×10^7 commercially available PBCA-MBs (SonoMAC-r, SonoMAC GmbH, Aachen, Germany) in 50 µl cell culture medium were added to the mixture and activated with fUS as described. The PBCA-MBs float up on the surface of the liquid in the well to ensure direct contact of the MBs with the cells (HUVEC on basolateral surface) or insert membrane (4T1 on apical surface). After treatment, the samples were kept in the staining solution for two more minutes and washed in PBS. The insert membrane was cut out and imaged using fluorescence microscopy at 10 × magnification (Axio Imager M2, Carl Zeiss Microscopy, Oberkochen, Germany). The area fractions of dextran were determined using the ImageJ software (ImageJ 1.53q, Wayne Rasband, National Institute of Health, USA) and normalized to the WGA signal. The different color channels were processed separately and the Otsu threshold method [41] was used to quantify the area fraction of intracellular dextran by creating a binary mask. Cell viability of the samples was confirmed by live/dead staining using fluorescein diacetate (5 mg/ml) and propidium iodide (2 mg/ml).

Cell layer integrity was assessed by TEER measurements and evaluation of 70 kDa dextran diffusion across the monolayer. TEER measurements were performed using an epithelial/ endothelial volt/ ohmmeter (EVOM2) with an STX4 electrode (World Precision Instruments Germany GmbH, Friedberg, Germany). MB-fUS treatment was performed in 300 µl cell culture medium mixed with 2×10^7 PBCA-MBs in 50 µl cell culture medium. The baseline TEER was acquired before the treatment and TEER was reassessed immediately after treatment and after two hours. The detected change in TEER was calculated as a percentage change, with the baseline considered as 100 %. TEER values were normalized to the growth area of the cell culture insert (0.33 cm^2), and the system blank was subtracted.

To assess the diffusion of 70 kDa dextran across the cell monolayer, cells were exposed to MB-fUS treatment as described above for TEER measurements. Subsequently, the cells were returned to the culture multiwell plate, and 100 µl Rhodamine B-labeled 70 kDa dextran solution (0.25 mg/ml in PBS) was added to the basolateral compartment and samples were placed back in the incubator. After 15 min and two hours, a 50 µl aliquot was taken from the apical compartment. The fluorescence intensity of the medium aliquots was measured using a Tecan plate reader at 570/590 nm (excitation/ emission), and the system blank was subtracted.

2.2. MB-fUS treatment of tumor-bearing mice

All animal experiments were conducted in compliance to the European Directive 2010/63 on the protection of animals for scientific purposes. The ethical committee of the governmental authority the German State Office for Consumer Protection and Food Safety (LAVE) North Rhine-Westphalia, Germany) formally approved the conduct of the described experiments (reference number: 80–02.04.2020.A204).

2.2.1. Tumor inoculation

Female Balb/cAnNRj mice aged 10 – 12 weeks (19 – 23 g) (Janvier Labs, Saint Berthevin, France) were housed in groups of 3 – 5 animals under specific pathogen-free conditions with a 12 h light/dark cycle. A temperature of 20 – 24 °C and a relative humidity of 45 – 65 % were maintained according to the guidelines of the "Federation for Laboratory Science Associations". Sterilized standard pellets and acidified water were provided ad libitum. Animals were left undisturbed for one week for acclimatization until enrolment in the experiment. All anesthetic procedures were performed using inhalation isoflurane anesthesia at 5 % for induction and 2 % for maintenance in oxygen-enriched air. All intravenous injections were performed in a lateral tail vein using 30 G catheters, which were flushed with 0.9 % sodium chloride (NaCl) solution before and after injections.

The syngeneic triple-negative mammary carcinoma 4T1 was inoculated into the right, fourth mammary fat pad by injection of 4×10^4 4T1 cells in 50 µl cell culture medium. The 4T1 cells were cultured over one week prior to injection and used when they reached approximately 70 % confluence. The mice were monitored daily, including tumor size measurements, using a caliper.

2.2.2. Extravasation of rhodamine B-labeled dextran

The aim of this experiment was to assess the influence of MB-fUS treatment on the permeability of tumor vessel walls by evaluating the extravasation of fluorescently labeled dextran. When the tumors reached a diameter of 4 – 6 mm, the experiment was started and MB-fUS treatment was compared with controls. Two cohorts were scheduled to assess the extravasation of dextran immediately after the treatment (day 0, Fig. 1 B.1) or two days after the treatment (day 2, Fig. 1 B.2). Thus, 20 mice were randomly assigned to four groups (using random numbers in Excel, n = 5 per group): MB-fUS (day 0), control (day 0), MB-fUS (day 2), and control (day 2). On day 0, both MB-fUS cohorts (day 0 and day 2) were subjected to MB-fUS treatment (Fig. 1 B.+B.2). Same number of control animals were scheduled and underwent only isoflurane anesthesia without application of the MB-fUS treatment.

MB-fUS treatment was performed using the same fUS system as previously described for the *in vitro* experiments. The US settings were identical to the *in vitro* experiments except for a prolonged exposure time of 1 min. The mouse was positioned in supine with the right hip slightly elevated to expose the tumor in the right groin. The fUS transducer was placed over the tumor at a distance of 25 mm from the tumor center to the transducer surface and the gap was closed with US gel. Concurrently with the fUS application, 1×10^8 PBCA-MBs (SonoMAC-r, SonoMAC GmbH, Aachen, Germany) in 50 µl PBS (equivalent to 2×10^9/ml) were injected intravenously. Mice in the cohort day 0 were euthanized on the same day after the respective treatment (Fig. 1 B.1) whereas animals in the day 2 cohort were kept for a further two days (Fig. 1 B.2).

Fifteen minutes before the euthanasia of each animal, 100 µl of Rhodamine B-labeled 70 kDa dextran (10 mg/ml in PBS) was injected intravenously to detect effects on vascular permeability. Additionally, 70 µl of fluorescein isothiocyanate (FITC)-labeled lectin was injected intravenously to visualize perfused vessels. Immediately before euthanasia of each animal, blood was collected retrobulbar and processed on the same day. Animals were euthanized by cervical dislocation and dissected, tumors removed and snap frozen in Tissue-Tek.

2.2.3. MB-fUS-assisted Doxil therapy

To evaluate the influence of MB-fUS treatment on the anti-cancer effect of a commercial chemotherapeutic agent (Doxil), 15 mice were randomly allocated to three different groups (n = 5 per group) using random numbers in Excel. When the tumors reached a diameter of 4 – 6 mm, therapy was initiated on day 0 and repeated on day 6, the experiment was terminated on day 10 (Fig. 1 C.1). The first group received intravenous injections of Doxil (2 mg/ml) at 5 mg/kg body weight combined with MB-fUS treatment (Doxil MB-fUS group) as explained in the previous section. In the second group, only Doxil (2 mg/ml, 5 mg/kg body weight) was injected intravenously (Doxil group). Mice of the third group received intravenous injections of 50 µl 0.9 % NaCl solution (NaCl group). Fifteen minutes before the euthanasia of each animal, 70 µl of FITC-labeled lectin was injected intravenously to detect perfused vessels. Animals were euthanized by cervical dislocation, tumors were excised and preserved in Tissue-Tek at – 80°C. Tumor volumes were calculated based on daily caliper measurements as volume = (length × width^2)/2, with the longest dimension applied as the length and all dimensions given in [mm].

2.3. Ex vivo analysis

2.3.1. Histological quantification of intra-tumoral dextran

To quantify the amount of extravasated dextran, 8 µm thick cryosections were prepared. The tumor sections were analyzed by fluorescence microscopy at 40 × magnification (N.A. = 0.95). For image acquisition, first, a perfused vessel (FITC-stained) was selected in the green channel to avoid bias, and then the signal of the dextran in the red channel was captured. Twenty images, obtained from two cryosections from the tumor center were evaluated per animal. The fluorescence intensity of dextran was analyzed using the Imalytics Preclinical software (Gremse-IT, Aachen, Germany) by segmenting the vessels in the image and defining three regions around the vessel at different distances (12, 24, and 36 µm). The fluorescence intensity was determined as a function of the distance from the nearest vessel. Vessel segmentation was based on the injected FITC-lectin, which binds to the endothelial cells in the vessel wall. The segmented area includes both the vessel wall and vessel lumen. Here it is important mentioning, that the vessels collapsed due to the blood withdrawal immediately before euthanasia, resulting in a negligible lumen space and the dextran quantified at the vessel was colocalized with FITC-lectin and the vessel wall. An example of the segmentation of the vessels and the definition of the three distances is shown in Fig. 2. A tumor section without dextran was imaged in the same way to correct for background noise and autofluorescence.

2.3.2. Detection of circulating tumor cells in mouse blood after MB-fUS treatment

In order to detect the appearance of circulating tumor cells in the blood after sonopermeation, an assay was performed according to a protocol previously published by Pulaski and colleagues [42]. Briefly, 500 µl mouse blood was diluted in 10 ml of Hank's Balanced Salt Solution and centrifuged at 1500 rpm for five minutes. The supernatant was then removed and this washing step was repeated. The remaining cell pellet was resuspended in 10 ml of cell culture medium (RPMI + 10 % FBS and 1 % P/S) supplemented with 60 µM of the cytostatic drug 6-thioguanine, to which 4T1 cancer cells are resistant. The cell suspension was transferred to a cell culture flask and left undisturbed in the incubator (37°C, 5 % CO_2 in a humidified atmosphere) for two weeks. After this time, the medium was replaced with PBS and 4T1 cell colonies were counted by bright field microscopy. As a positive control, 4T1 cells seeded in 6-well plates (n = 9) were cultured with the same medium and a lactate dehydrogenase assay was performed to assess viability.

2.3.3. Histological analysis of tumor vessels after dextran extravasation

For histological analysis of tumor tissue, 8 µm thick cryosections were immunohistologically stained. The tumor vasculature was stained using a CD31 antibody to determine the absolute number of vessels. The fraction of perfused vessels was analyzed as the percentage of vessels stained with FITC-lectin of all CD31-stained vessels. Analyses were performed on 15 fluorescence microscopy images per animal using ImageJ. A detailed description of the antibodies and staining protocol is provided in supplementary data Tables S1 and S2.

2.3.4. Histological analysis of Doxil therapy outcome

Cryosections of 8 µm in thickness were used to detect microscopic changes in the tumor tissue after the Doxil therapy. We analyzed the tumor vasculature (CD31), macrophage infiltration (F4/80), apoptotic activity (active Caspase 3), tumor cell proliferation (KI67), and remodelling of the tumor microenvironment (VEGF and MMPs). A detailed description of the antibodies and staining protocol can be found in supplementary Tables S1 and S2. In total, 15 fluorescence images (five different cryosections and three images per section) were analyzed per tissue marker and mouse using ImageJ software. The red channel with the respective marker was processed separately from the others and the Otsu threshold method [41] was applied to determine the area.

2.4. Statistical analysis

Statistical analyses were performed using GraphPad Prism (Version 10.5.0). Data are expressed as mean ± standard deviation. Normal distribution was confirmed by applying the Kolmogorov-Smirnov and Shapiro-Wilk test. One-way or two-way ANOVA combined with the Tukey's test were used to check for statistical significance. Statistical significance was defined as a p-value ≤ 0.05.

3. Results

3.1. Sonoporation and sonopermeation of HUVEC and 4T1 cells

HUVEC monolayers were seeded on the basolateral surface of cell culture inserts and upon exposure to MB-fUS treatment, sonoporation and sonopermeation effects were observed. Sonoporation of the cell membrane resulted in a significant cellular uptake of Rhodamine B-labeled 70 kDa dextran compared to sham-treated control samples (Fig. 3 A+B). Sonopermeation of the cell layer was investigated by TEER measurements and diffusion of Rhodamine B-labeled 70 kDa dextran across the cell monolayer. MB-fUS exposure induced a significant decrease in TEER (Fig. 3 C) and a significant increase in the amount of diffused dextran compared to control samples (Fig. 3 D). Two hours after the treatment, TEER and dextran diffusion were reassessed on the same samples and showed no significant differences from control samples (Fig. 3 C+D), indicating recovery of the cell monolayer.

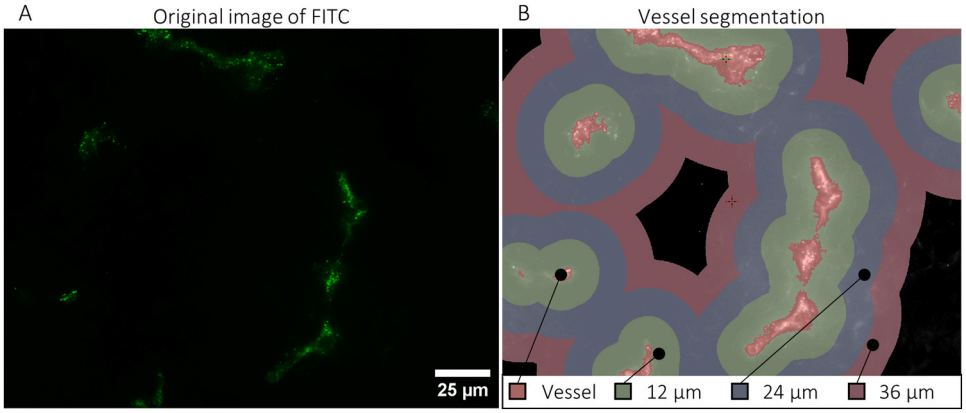

Fig. 2. Example segmentation of FITC-lectin-stained blood vessels. A. Original fluorescence image of FITC-lectin-stained blood vessels. B. Segmentation of blood vessels shown in A based on FITC-lectin signal. Three regions at defined distances (12, 24 and 36 µm) from the vessels are visualized and used to evaluate fluorescence intensity of dextran dependent on the distance from the vessel.

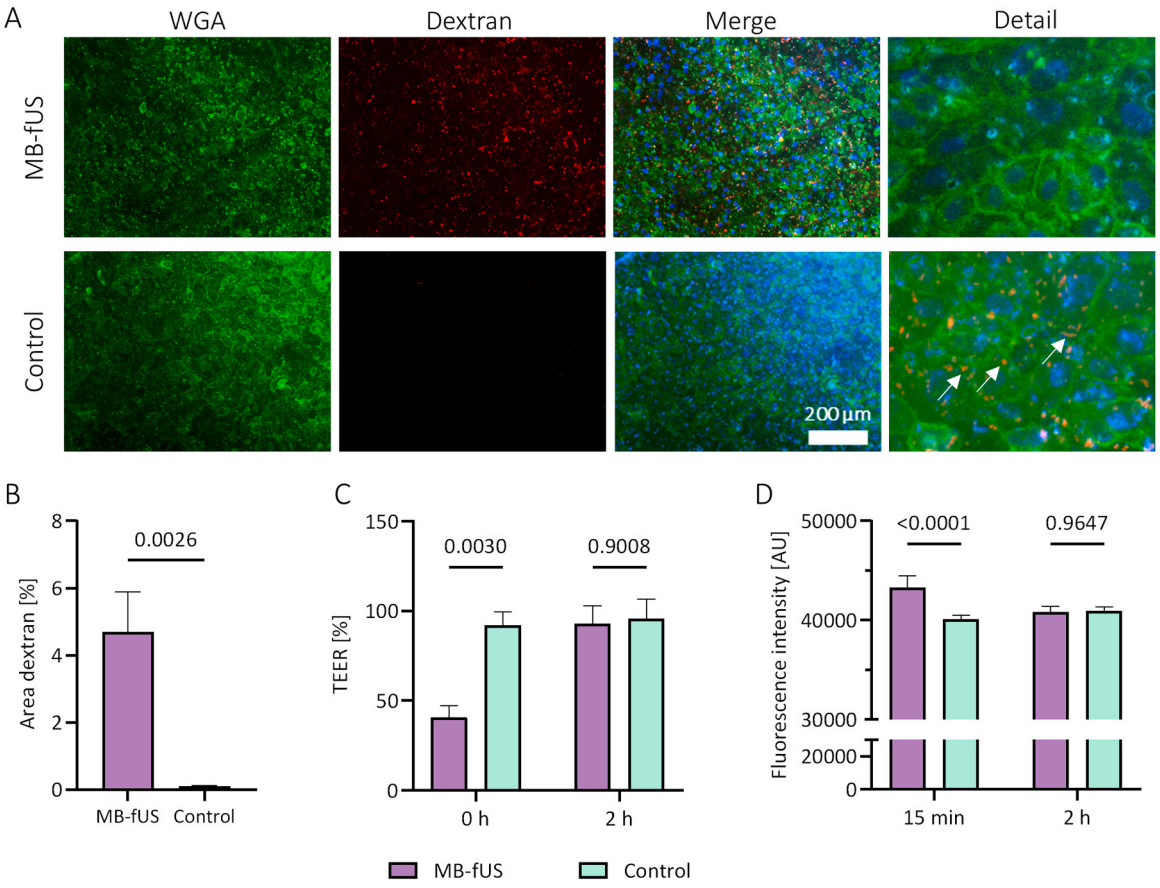

Fig. 3. *In vitro* sonoporation and sonopermeation of HUVEC monolayers. A. Representative fluorescence images of HUVEC monolayers exposed to microbubble-assisted focused ultrasound (MB-fUS) treatment or sham treatment (control). Cell nuclei and cell membranes were stained with Hoechst (blue) and wheat germ agglutinin (WGA, green), respectively, and sonoporation was visualized with Rhodamine B-labeled 70 kDa dextran (red). MB-fUS treated sample displays multiple small red dots corresponding to intracellular dextran. B. Quantified area fractions of intracellular dextran reveal significantly more dextran incorporated into cells after MB-fUS treatment compared to controls. C. MB-fUS treatment results in significantly lower transendothelial electrical resistances (TEER) immediately after exposure as compared to sham treatment. TEER values appear to recover within two hours. D. The diffusion assay shows enhanced diffusion of dextran across the cell monolayer after MB-fUS treatment compared to the control group. Reassessment of the diffusion two hours after the treatment shows no significant difference. Data are expressed as mean ± standard deviation of n = 3.

After evaluating the effects on a HUVEC monolayer, we also evaluated effects on a monolayer of 4T1 cancer cells. Here, we advanced the setup, by creating an artificial barrier (insert membrane) between the 4T1 cells and the PBCA-MBs, increasing the distance between the cell monolayer and the PBCA-MBs by seeding the 4T1 cells on the opposite side of the cell culture insert membrane. While for HUVEC on the basolateral surface, the PBCA-MBs were in direct contact to them, 4T1 cells on the apical side, were separated from the MBs by the insert membrane (refer to Fig. 1 A1 +A2). With this adapted experimental setup, we approached the actual situation in the tumor, where the MBs are constrained to the blood vessels. The experiments revealed significant sonoporation effects on 4T1 cells after MB-fUS treatment (Fig. 4A+B), as well as reduced layer integrity due to sonopermeation (Fig. 4C+D) compared to sham-treated control samples. Sonopermeation effects appeared to restore within two hours, when effects were reassessed.

We have additionally validated the biological effects in HUVEC and 4T1 cell monolayers after MB-fUS treatment at a lower acoustic pressure (300 kPa). Next to that, we investigated whether lower PBCA-MBs concentrations can induce (1×10^7 and 5×10^6) significant biological effects. Moreover, we evaluated the change in TEER after MB-fUS exposure using a murine endothelial cell line (2H-11). The corresponding results are supplemented in Figures S1 and S2.

In both cell lines, viability at 600 kPa was assessed by a live/dead staining using propidium iodide (2 mg/ml) and fluorescein diacetate (5 mg/ml). Hardly any dead cells were detected indicating that our intervention was tolerated by the cells (supplementary Figure S3).

3.2. Enhanced in vivo extravasation of dextran after MB-fUS exposure

To assess whether MB-fUS treatment increases tumor vessel permeability, 4T1 tumor-bearing mice were injected with Rhodamine B-labeled 70 kDa dextran 15 min before euthanasia. Dextran leakage into the tumor tissue (extravasation) was measured at two time points: immediately after treatment and two days later.

MB-fUS application to tumors promoted significantly higher levels of dextran at the tumor vessels (colocalized with the segmented area, based on FITC-lectin) immediately after the treatment (day 0) compared to control animals. Additionally, the analysis demonstrated that significantly more dextran extravasated into the tumor tissue 12 and 36 µm from the vessel immediately after MB-fUS exposure (Fig. 5A). Two days after MB-fUS treatment, tumors displayed significantly more dextran at the vessels compared to the control group (Fig. 5B, bottom), but the amount of extravasated dextran was not significantly different between both experimental groups (Fig. 5B).

The tumor vasculature was examined (representative fluorescence images in Fig. 6C) by determining the number of vessels (CD31) and the percentage of perfused vessels (FITC-lectin/CD31). The absolute number of tumor vessels was comparable between the groups (Fig. 6A). The percentage of perfused vessels tended to decrease directly after MB-fUS

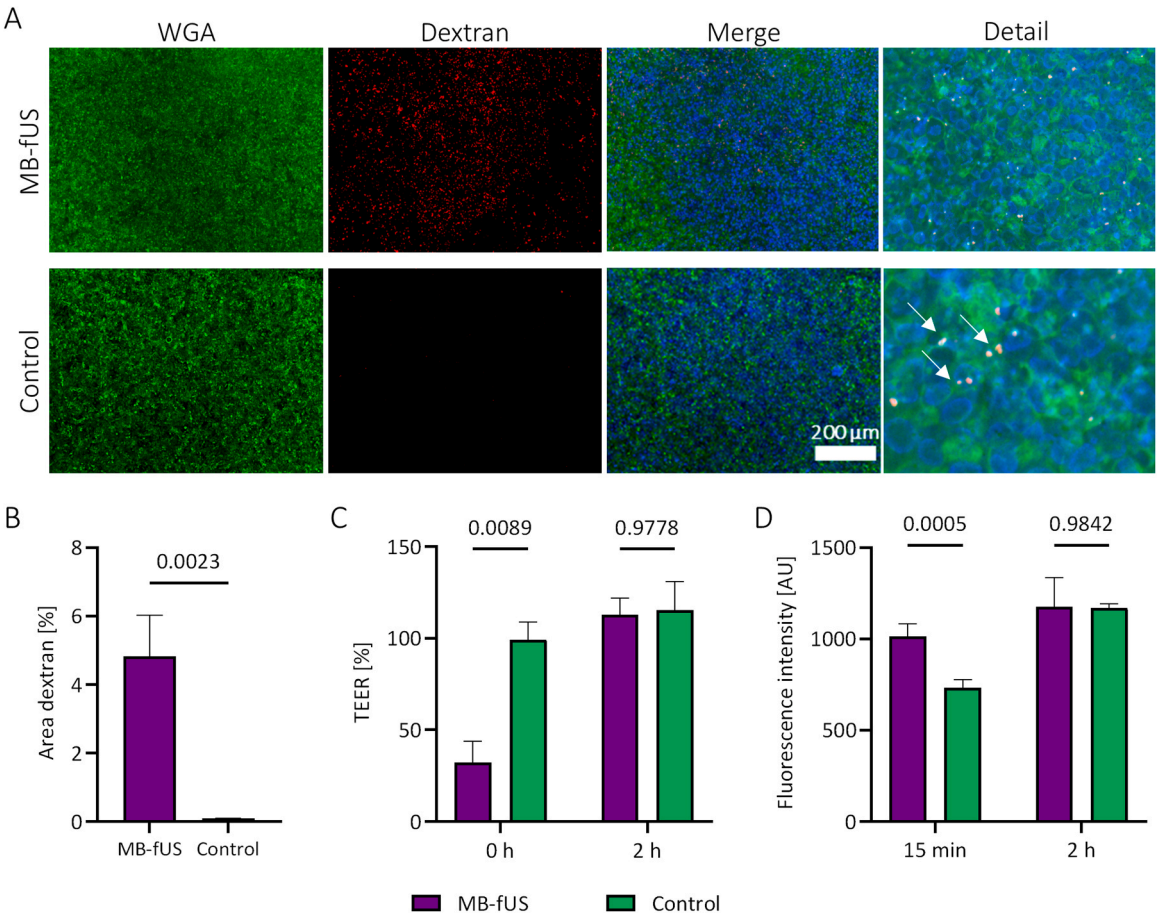

Fig. 4. *In vitro* sonoporation and sonopermeation of 4T1 monolayers. A. Representative fluorescence images of 4T1 monolayers treated with microbubble-assisted focused ultrasound (MB-fUS) or sham treatment (control) show intracellular Rhodamine B-labeled 70 kDa dextran (red) because of sonoporation. Cell nuclei were visualized with Hoechst (blue) and cell membranes with wheat germ agglutinin (WGA, green). B. MB-fUS treated samples present significantly more dextran incorporated into cells after MB-fUS treatment than sham-treated controls. C. Transendothelial electrical resistance (TEER) is significantly decreased immediately after MB-fUS application as compared to the controls. TEER values appear to restore within two hours. D. MB-fUS treatment results in enhanced diffusion of dextran across the cell monolayer compared to the control group. Reassessment of the diffusion two hours after the treatment shows no significant difference. Data are expressed as mean ± standard deviation of n = 3.

treatment than in the control group on day 0 and showed comparable values after 2 days (Fig. 6B).

3.3. Absence of circulating tumor cells after MB-fUS treatment

Blood of mice was collected immediately before euthanasia and processed to check for circulating tumor cells that might have escaped into the vasculature due to vascular permeabilization by MB-fUS treatment. After incubation of the cell pellet with 6-thioguanine for two weeks, no 4T1 cell colonies were found, pointing out that MB-fUS treatment did not induce tumor cell entry into the blood circulation and thus did not increase the risk of metastasis. Resistance of 4T1 cells to 6-thioguanine was confirmed by a lactate dehydrogenase assay (results are shown in supplementary Figure S4).

3.4. Augmented anti-tumor effect of a low-dose Doxil treatment

Doxil treatment of 4T1 tumors was combined with MB-fUS (Doxil MB-fUS) to assess whether sonopermeation with PBCA-MBs enhances the therapeutic effect of Doxil. The control groups received either Doxil or 0.9 % NaCl injections both without MB-fUS. The tumor volumes were assessed daily for ten days after the first treatment on day 0, which was repeated on day 6. On day 6, one mouse in the Doxil group had to be removed from the experiment, and data of this animal are included until day 6. Evaluation of the absolute tumor volumes showed an initial increase in tumor size in all three groups after the first treatment. After the second treatment, the tumors continued to grow in both the Doxil and NaCl groups, as shown in Fig. 7A. By contrast, tumor growth was hampered in the Doxil MB-fUS treated group. The final tumor volumes, shown in Fig. 7B, point to a tendency of tumor volume decrease in the Doxil group but a strongly enhanced effect when combined with MB-fUS.

To detect histological changes in the tumor tissue, we investigated the tumor vessels (CD31), macrophage infiltration (F4/80), apoptotic activity (active Caspase 3), and tumor cell proliferation (KI67). Area fractions of the different tissue markers were quantified and revealed that Doxil and Doxil MB-fUS treated mice had fewer vessels compared to the NaCl control group (Fig. 8A), which can be explained by the cytotoxic effect of Doxil. The presence of F4/80$^+$ macrophages was significantly lower in the Doxil MB-fUS group and the Doxil group compared to the NaCl group. Furthermore, Doxil MB-fUS tumors contained significantly less F4/80$^+$ macrophages than Doxil-treated tumors (Fig. 8B). Increased apoptosis (active Caspase 3, Fig. 8C) and lower cancer cell proliferation (KI67, Fig. 8D) further confirmed the higher therapeutic efficacy of the Doxil MB-fUS treatment compared to Doxil treatment alone. Apoptosis was not enhanced by Doxil treatment alone compared to NaCl, while cancer cell proliferation was significantly reduced. These findings are further corroborated by our findings on changes in the tumor microenvironment. We have additionally analyzed vascular endothelial growth factor protein A (VEGF) as well as presence of active

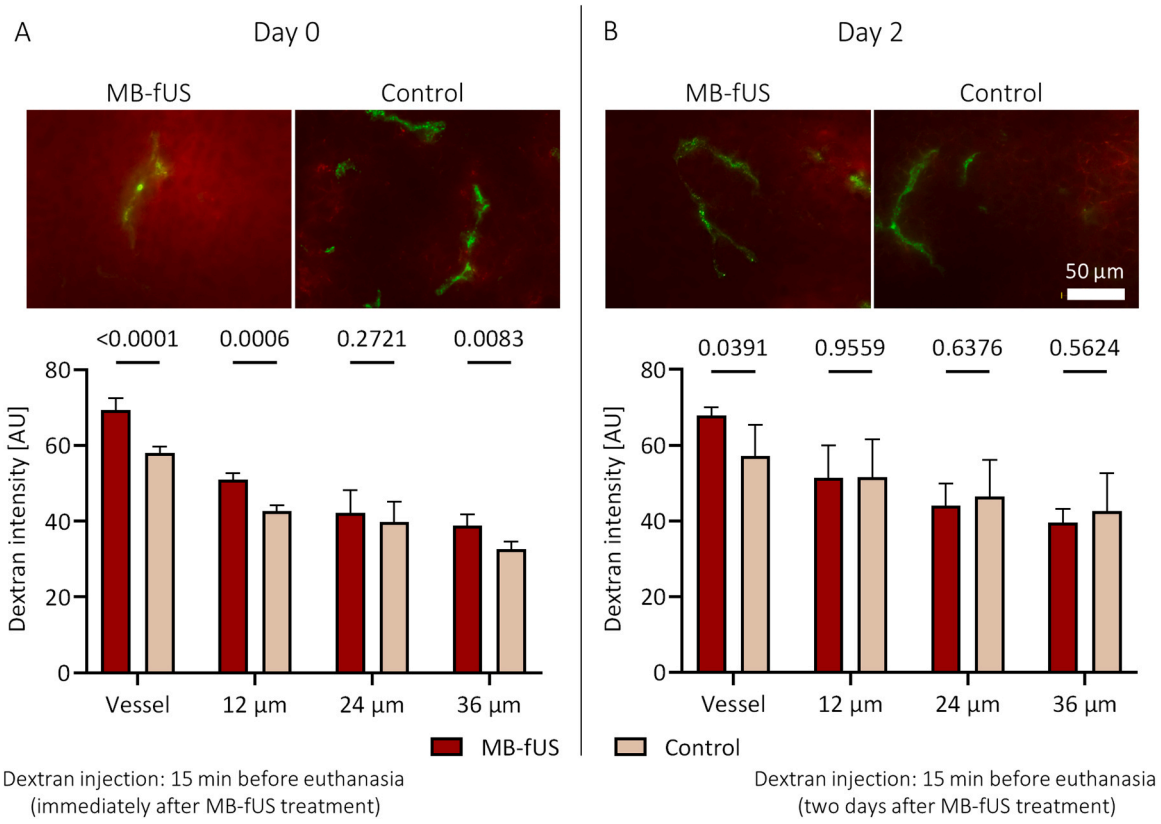

Fig. 5. Dextran extravasation in 4T1 tumors of mice after MB-fUS. Dextran was injected 15 min before the euthanasia of each animal A. Data of day 0 cohort, euthanasia immediately after treatment. The left image shows a tumor section of a microbubble and focused ultrasound (MB-fUS) treated tumor with more red fluorescence (dextran) around perfused tumor vessels (green) compared to the control sample (right). The quantification of fluorescence intensities of dextran in the tumor tissue reveals significantly more dextran at the tumor vessels and at distances of 12 and 36 µm from the vessels after MB-fUS treatment. B. Data of day 2 cohort, euthanasia two days after treatment. Dextran fluorescence intensity is significantly higher at the tumor vessels of the MB-fUS treated group but not in the extravascular tissue. Data are expressed as mean ± standard deviation of n = 5.

matrix metalloproteinases (MMPs, gelatinases and collagenases) (data shown in supplementary figure 5). For Doxil MB-fUS treated tumors, we found a significant downregulation in expression of VEGF and reduced activity of MMPs compared to Doxil and NaCl groups.

4. Discussion

In this study, we investigated whether PBCA-MB-assisted fUS treatment enhances the therapeutic potential of Doxil in treating murine breast cancer. In this regard, we demonstrated that MB-fUS treatment with PBCA-MBs induces sonoporation and sonopermeation in HUVEC and 4T1 monolayers. *In vivo,* sonopermeation with PBCA-MBs increased vascular permeability and the extravasation of 70 kDa dextran into the tumor tissue. Additionally, PBCA-MB-aided sonopermeation significantly improved the therapeutic efficacy of Doxil in murine breast cancer tumors by inhibiting tumor growth.

In our previous study, we characterized the US response of PBCA-MBs at 1 MHz and reported mixed non-destructive and destructive PBCA-MB responses at *in situ* PNPs of 500 and 665 kPa [30]. Furthermore, compression-only and compression-dominated behavior were found during non-destructive responses, which are termed "compression-driven responses" in this manuscript. The experiments indicated that both compression-driven non-destructive responses and destructive responses were capable of inducing biological effects *in vitro* [30], emphasizing the unique response profile of the PBCA-MBs. Based on these previous findings, we assume that, for the *in vitro* experiments in this study, the PBCA-MBs underwent both compression-driven non-destructive responses and destructive responses when an *in situ* PNP of 600 kPa was applied. Therefore, we conclude that the sonoporation and sonopermeation effects were because of the exertion of stress onto the cells by a synergistic effect of mixed MB responses. In line with results from De Cock *et al.* [43], we found that sonoporation resulted in enhanced endocytosis of dextran into the cytoplasm, as indicated by the characteristic punctate pattern of endocytic pockets. Besides this, sonopermeation experiments led to a reduced cell layer integrity. This might be due to the opening of cell-cell contacts or the formation of transcellular tunnels, as proposed by literature [44–47]. The baseline TEER values of HUVEC and 4T1 cells (HUVEC: 25.5 ± 3.9 Ω^*cm^2, 4T1: 22.6 ± 2.3 Ω^*cm^2) were in the range of similar cell monolayers [48–51].

Previous studies have reported the bubble-to-cell distance to be a critical determinant of sonoporation efficiency [52]. The 4T1 and HUVEC monolayers were cultured on the apical and basolateral surfaces of cell culture inserts, respectively. The different locations of the cells on the insert membrane resulted in a larger cell-to-bubble distance for the 4T1 monolayers due to the several micrometer thick [53] insert membrane, separating the cells and MBs. The setup more closely represents the situation *in vivo*, where MBs are intravascular and are separated from the extravascular tumor tissue by the vessel walls. Notably, the different locations did not affect sonoporation or sonopermeation effects, which were similar for the two cell types, indicating that such effects on endothelial cells or cells outside the vasculature are possible with our protocol. For the *in vitro* setting using the cell culture insert, we suppose that effects by the responding PBCA-MBs were conveyed across the membrane, most likely via pores in the membrane that potentially channeled the induced liquid motions by the MBs.

Subsequently, the same US settings were used for the *in vivo* MB-fUS treatment of murine tumors. However, the attenuation of US by the skin

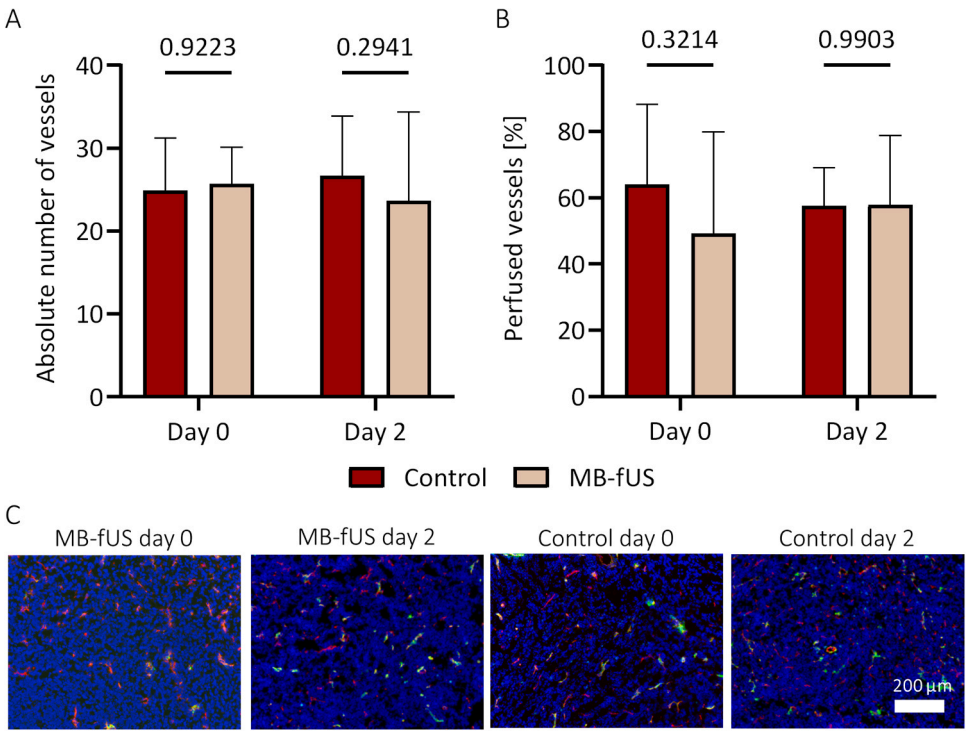

Fig. 6. Tumor vasculature perfusion assessment. A. The absolute number of tumor vessels based on CD31 staining shows no significant differences between the different groups. B. The percentage of perfused vessels is slightly lower on day 0 directly after microbubble and focused ultrasound (MB-fUS) treatment, whereas on day 2, values are comparable. C. Representative fluorescence images of tumor cryosections showing perfused (green) and all vessels (red). Nuclei were counterstained with DAPI (blue). Results are presented as mean ± standard deviation of n = 5.

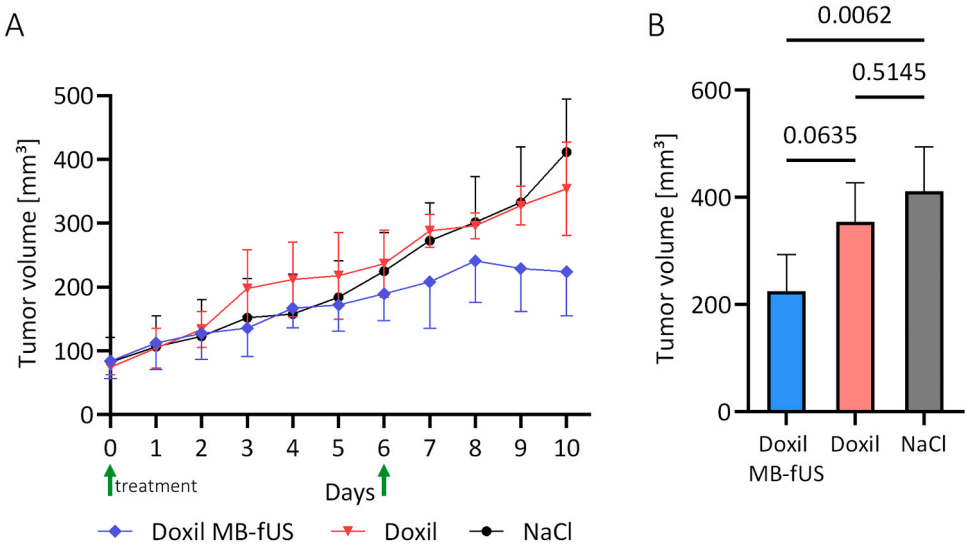

Fig. 7. Evaluation of the tumor volume change. One mouse from the Doxil group had to be removed from the experiment on day 6, the respective data are included until day 6. A. Tumor volumes continuously increase in the Doxil and NaCl groups throughout the observation period. Doxil MB-fUS treatment hampers tumor growth after the second treatment. Group-specific treatments were administered on days 0 and 6, as indicated by green arrows. B. Final tumor volumes on day 10 highlight that tumors in the Doxil MB-fUS treated mice were smaller than tumors in the Doxil and NaCl groups. Doxil alone only slightly reduced tumor volumes. Results are presented as mean ± standard deviation of n = 5, except for Doxil group, see earlier note on group size.

of the mice had to be considered, for which an attenuation of 11.3 % at 2.25 MHz has been reported [54]. As US attenuation decreases at lower frequencies [55], we estimated that, in our experiments with a driving frequency of 1 MHz, the intra-tumoral PNP was still above 500 kPa. Thus, based on the previous data discussed above [30], we assume that PBCA-MBs in the tumor vasculature exhibited both non-destructive and destructive responses.

The dextran extravasation study demonstrated that MB-fUS treatment affected the integrity of the vessel walls and enhanced extravasation. In this context, dextran was administered directly after as well as two days after the MB-fUS treatment (15 min before euthanasia). In both cases, we found more dextran at the tumor vessels, which most likely is related to enhanced endothelial uptake, *e.g.* due to enhanced endocytic activity, as observed in our *in vitro* experiments. In addition, we detected

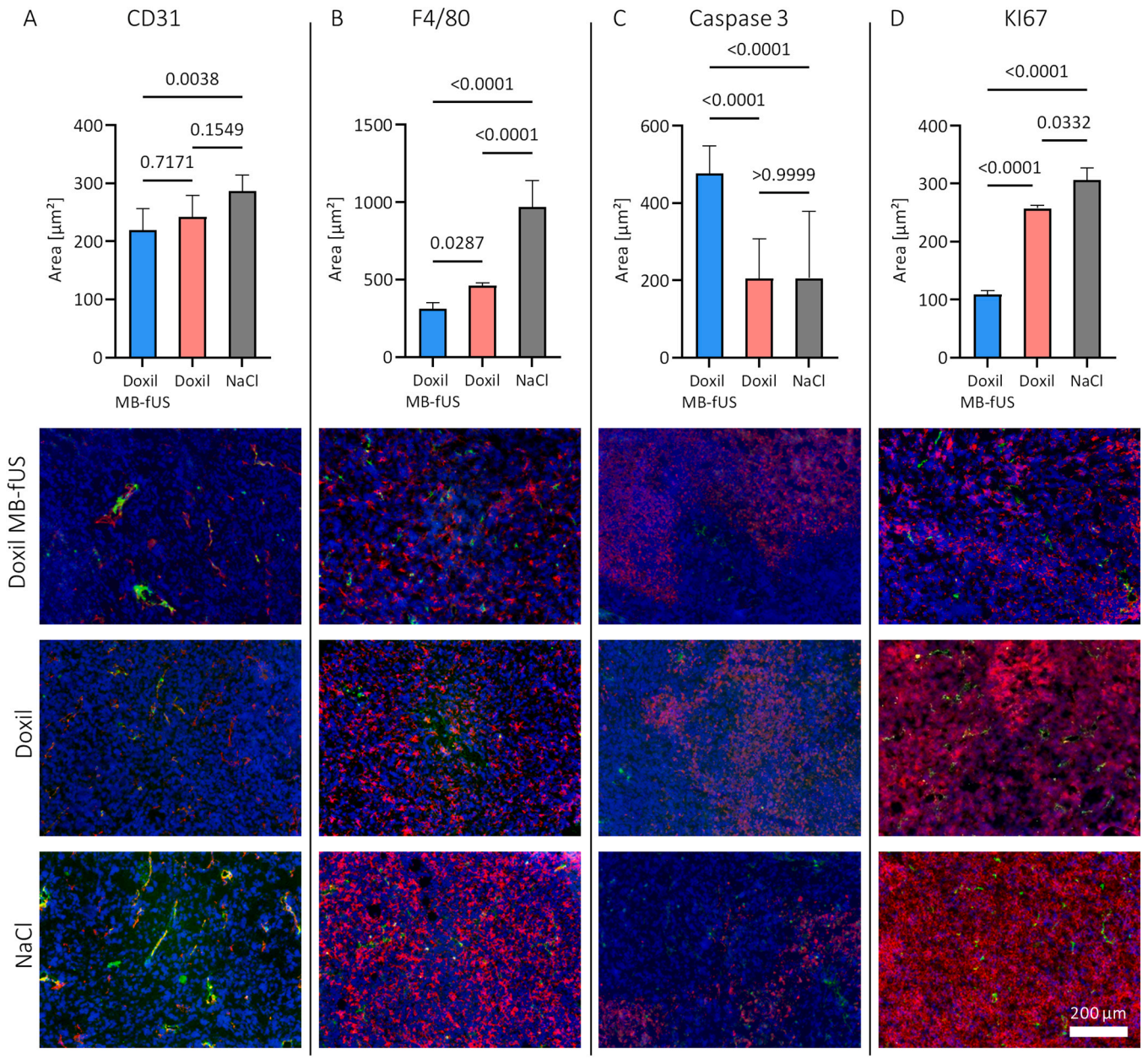

Fig. 8. Histological analysis of tumor cryosections. A. CD31 staining shows that the Doxil MB-fUS group had the smallest area fraction of CD31, which is significantly smaller compared to the NaCl control group. B. Murine macrophages ($F4/80^{+}$) are significantly reduced in the Doxil MB-fUS group than in the Doxil group, as well as compared to the NaCl group. The Doxil group displays significantly less $F4/80^{+}$ signal than the NaCl group. C. Caspase 3 staining revealed significantly higher apoptosis in the Doxil MB-fUS group compared to both the NaCl and Doxil-treated groups, respectively. D. Cancer cell proliferation (KI67) is significantly lower in the Doxil MB-fUS group than in the Doxil and NaCl control groups, respectively. Results are expressed as mean ± standard deviation of n = 5, except Doxil group, see earlier note.

more extravascular dextran, when it was administered immediately after MB-fUS, suggesting that MB-fUS treatment increased the vascular permeability potentially by opening inter-endothelial junctions and untightening the extravascular matrix, as hypothesized by Theek *et al.* [37]. In this regard, the disruption and disorientation of collagen fibers after application of MB-fUS [56] might play a crucial role in loosening the extracellular matrix to increase penetration depth of drug carriers by MB-fUS as previously confirmed in other studies [57–59]. In contrast, when dextran was administered two days after the MB-fUS, no effect on the extravascular amount of dextran was found, suggesting that the biological barriers (endothelial layer and extracellular matrix) had largely closed again. A potential explanation for this might be the greater distance of PBCA-MBs to the extravascular tissue as compared to the vessel wall, since the MBs are constrained to the tumor vessel and not in direct contact with the tumor tissue itself. This difference might result in a weakening of the effects on extravascular tissue. Furthermore, we found a slightly reduced perfusion immediately after MB-fUS treatment, whereas, two days after the treatment, no effect on tumor perfusion was detected. While less perfusion would also result in less dextran accumulation, as reported for chemotherapeutics [60], acute vascular damage also goes along with higher leakiness. These two effects can partially compensate for each other, and thus, it is important to ensure that sonoporation and sonopermeation effects dominate the vascular ablation, as it was the case in our setting. Previous studies have also reported the shutdown of blood flow associated with minor endothelial cell damage. The blood flow was then restored within a maximum of 30 min

[61,62]. In our experiment, the mice were euthanized 15 min after treatment, which was presumably not enough time for blood flow to be restored.

Having confirmed enhanced dextran extravasation after MB-fUS treatment, we explored the effect of the MB-fUS treatment on a Doxil therapy in 4T1 tumor-bearing mice. For this purpose, we selected a dosage of Doxil that typically does not significantly inhibit tumor growth [63–66]. We demonstrated that combining Doxil therapy with our MB-fUS protocol significantly improved tumor response and hampered tumor growth, as indicated by increased apoptosis (Caspase 3), reduced cancer cell proliferation (KI67) and reduced expression of VEGF and activity of MMPs, indicating slowed-down angiogenesis and hampered tumor progression. We hypothesize that more Doxil was available in MB-fUS-treated tumors, most likely due to increased vascular permeability allowing more Doxil to accumulate in the tumor. Apart from this effect, macrophages carrying Doxil and residing in the tumor may also have contributed to the improved tumor response. It has been reported that macrophages act as depot for nanomedicines [67]. Upon cellular uptake, the liposomal shell of Doxil is degraded, releasing the enclosed doxorubicin and killing the macrophages. As a consequence, free doxorubicin is released by the macrophages and easily diffuses into adjacent cancer cells [67]. Our histological analysis of the tumor tissue corroborates this theory, showing that less macrophages were found in Doxil-treated tumors than in the NaCl group. This effect was enhanced when Doxil therapy was combined with MB-fUS, suggesting that more Doxil was available.

A limitation to the generalizability of the study is that it did not consider gender/sex issues. Further, we did not find a reduction in tumor growth immediately after the first administration of Doxil MB-fUS. A potential explanation for this slight delay might be that initial effects on tumor growth were only visible on a microscopic level and thus were not immediately reflected on a macroscopic basis. Next to that, macrophages internalizing the Doxil particles and afterwards acting as a drug reservoir [67] might also decelerate the chemotherapeutic effect.

Based on our *in vivo* findings, we infer that our MB-fUS protocol with a PNP of 600 kPa, resulted in a synergistic combination of both non-destructive and destructive responses of PBCA-MBs. The US-activated PBCA-MBs induced the intended biological effects without causing vascular ablation; thus, the mixed responses appear to be a beneficial compromise of both response regimes. Previous studies using PBCA-MBs have confirmed their safe use *in vivo* in different animal models [31,33,34,68] and showed promising performance for diagnostic purposes [32,69] as well as in the permeabilization of the blood-brain barrier [35] and peripheral tumors [37]. In the present study, we confirmed their therapeutic potential to improve the tumor response without causing adverse effects in a preclinical setting that supports paving the way for clinical applications. The adjustable size distribution contributes to advancing robustness and reproducibility of sonopermeation protocols, making these interventions more efficient and safer. This renders PBCA-MBs a relevant candidate for clinical use.

Although 70 kDa dextran and Doxil differ in size (2 – 3 nm vs. ≈100 nm) [70,71], our MB-fUS protocol increased vascular permeability for both nanomedicines. However, it has to be taken into account that the 4T1 breast cancer model is characterized by immature and leaky vessels, which contain little connective tissue [23]. Human tumor vessels often deviate from that and show high levels of collagen [23]. Varying amounts of connective tissue need to be taken into consideration when adjusting the US parameters because higher collagen deposition may weaken the mediated effects. For this reason, future work will validate our MB-fUS protocol with the PBCA-MBs in tumor models with a more mature vasculature and different desmoplastic levels [72].

5. Conclusion

We showed that with PBCA-MB-assisted fUS treatment, we can induce biological effects in facilitating drug delivery of dextran in both *in vitro* and *in vivo* scenarios. Our approach has resulted in enhanced vascular permeability and increased intra-tumoral accumulation of dextran. To demonstrate the clinical relevance of our findings, for the first time, we demonstrated that MB-fUS treatment using PBCA-MBs increased the therapeutic effect of a clinically-approved nanomedicines drug (liposomal doxorubicin, Doxil), showcasing its potential for improved tumor response in future sonopermeation interventions.

CRediT authorship contribution statement

Julia Blöck: Writing – original draft, Visualization, Investigation, Formal analysis, Data curation. **Lea Imschweiler:** Writing – review & editing, Investigation. **Rahaf Mihyar:** Writing – review & editing, Formal analysis. **Junlin Chen:** Formal analysis, Investigation, Writing – review & editing. **Roman Barmin:** Writing – review & editing, Investigation. **Susanne Koletnik:** Writing – original draft, Investigation. **Roger M. Pallares:** Writing – review & editing. **Twan Lammers:** Writing – review & editing, Resources, Funding acquisition. **Anne Rix:** Writing – review & editing, Supervision, Methodology, Conceptualization. **Fabian Kiessling:** Writing – review & editing, Supervision, Resources, Methodology, Funding acquisition, Conceptualization.

Declaration of Competing Interest

The authors declare the following competing financial interest(s): T. L., A.R. and F.K. are among the co-founders of the SonoMAC GmbH that produces polymeric microbubbles.

Acknowledgements

The authors gratefully acknowledge financial support by the German Research Foundation (DFG GRK 2375 (Project No. 331065168))

Appendix A. Supporting information

Supplementary data associated with this article can be found in the online version at doi:10.1016/j.phrs.2025.107916.

Data availability

Data will be made available on request.

References

[1] S. Hernot, A.L. Klibanov, Microbubbles in ultrasound-triggered drug and gene delivery, Adv. Drug Deliv. Rev. 60 (2008) 1153–1166, https://doi.org/10.1016/j.addr.2008.03.005.
[2] J. Yoo, D. Heo, Y. Hwang, C. Kim, B. Park, Ultrasound-Mediated membrane modulation for biomedical applications, Nanomaterials 15 (2025) 884, https://doi.org/10.3390/nano15120884.
[3] A. Bouakaz, J. Michel Escoffre, From concept to early clinical trials: 30 years of microbubble-based ultrasound-mediated drug delivery research, Adv. Drug Deliv. Rev. 206 (2024) 115199, https://doi.org/10.1016/j.addr.2024.115199.
[4] J.M. Escoffre, N. Sekkat, E. Oujagir, S. Bodard, C. Mousset, A. Presset, R. Chautard, J. Ayoub, T. Lecomte, A. Bouakaz, Delivery of anti-cancer drugs using microbubble-assisted ultrasound in digestive oncology: from preclinical to clinical studies, Expert Opin. Drug Deliv. 19 (2022) 421–433, https://doi.org/10.1080/17425247.2022.2061459.
[5] S. Snipstad, K. Vikedal, M. Maardalen, A. Kurbatskaya, E. Sulheim, C. de, L. Davies, Ultrasound and microbubbles to beat barriers in tumors: improving delivery of nanomedicine, Adv. Drug Deliv. Rev. 177 (2021) 113847, https://doi.org/10.1016/j.addr.2021.113847.
[6] X. Lin, L. Cai, X. Cao, Y. Zhao, Stimuli-responsive silk fibroin for on-demand drug delivery, Smart Med. 2 (2023) 1–16, https://doi.org/10.1002/smmd.20220019.
[7] K. Chan, M. Saltagi, K.Y. Choi, The emerging role of sentinel lymph node biopsy in oral cavity and oropharyngeal carcinomas, Plast. Aesthetic Res. (2024), https://doi.org/10.20517/2347-9264.2023.79.
[8] K. Elumalai, S. Srinivasan, A. Shanmugam, Review of the efficacy of nanoparticle-based drug delivery systems for cancer treatment, Biomed. Technol. 5 (2024) 109–122, https://doi.org/10.1016/j.bmt.2023.09.001.

[9] K. Kooiman, S. Roovers, S.A.G. Langeveld, R.T. Kleven, H. Dewitte, M.A. O'Reilly, J.M. Escoffre, A. Bouakaz, M.D. Verweij, K. Hynynen, I. Lentacker, E. Stride, C. K. Holland, Ultrasound-Responsive cavitation nuclei for therapy and drug delivery, Ultrasound Med. Biol. 46 (2020) 1296–1325, https://doi.org/10.1016/j.ultrasmedbio.2020.01.002.

[10] S. Snipstad, E. Sulheim, C. De Lange Davies, C. Moonen, G. Storm, F. Kiessling, R. Schmid, T. Lammers, Sonopermeation to improve drug delivery to tumors: from fundamental understanding to clinical translation, Expert Opin. Drug Deliv. 15 (2018) 1249–1261, https://doi.org/10.1080/17425247.2018.1547279.

[11] M. Cattaneo, G. Guerriero, G. Shakya, L.A. Krattiger, L. G. Paganella, M.L. Narciso, O. Supponen, Cyclic jetting enables microbubble-mediated drug delivery, Nat. Phys. 21 (2025) 590–598, https://doi.org/10.1038/s41567-025-02785-0.

[12] C. Einen, S. Snipstad, H.F. Wesche, V. Nordlund, E.J. Devold, N. Amini, R. Hansen, E. Sulheim, C. de, L. Davies, Impact of the tumor microenvironment on delivery of nanomedicine in tumors treated with ultrasound and microbubbles, J. Control. Release 378 (2025) 656–670, https://doi.org/10.1016/j.jconrel.2024.12.037.

[13] B. Yousefian, S.M. Firoozabadi, M. Mokhtari-Dizaji, Sonochemotherapy of breast adenocarcinoma: an experimental in vivo model, J. Ultrasound 18 (2015) 165–171, https://doi.org/10.1007/s40477-014-0120-7.

[14] S. Snipstad, S. Berg, Ý. Mørch, A. Bjørkøy, E. Sulheim, R. Hansen, I. Grimstad, A. van Wamel, A.F. Maaland, S.H. Torp, C. de, L. Davies, Ultrasound improves the delivery and therapeutic effect of Nanoparticle-Stabilized microbubbles in breast cancer xenografts, Ultrasound Med. Biol. 43 (2017) 2651–2669, https://doi.org/10.1016/j.ultrasmedbio.2017.06.029.

[15] T.Y. Wang, J.W. Choe, K. Pu, R. Devulapally, S. Bachawal, S. Machtaler, S. M. Chowdhury, R. Luong, L. Tian, B. Khuri-Yakub, J. Rao, R. Paulmurugan, J. K. Willmann, Ultrasound-guided delivery of microRNA loaded nanoparticles into cancer, J. Control. Release 203 (2015) 99–108, https://doi.org/10.1016/j.jconrel.2015.02.018.

[16] M. He, X. Chen, F. Yu, B. Qin, H. Wang, L. Lavery, F.S. Villanueva, Enhanced antitumor efficacy and reduced cardiotoxicity of Ultrasound-Mediated doxorubicin delivery by Microbubble-Liposome complexes, Ultrasound Med. Biol. 51 (2025) 1240–1249, https://doi.org/10.1016/j.ultrasmedbio.2025.04.010.

[17] Y.J. Qiu, J.Y. Cao, J.H. Liao, Y. Duan, S. Chen, R. Cheng, Y.L. Huang, X.Y. Lu, J. Cheng, W.P. Wang, Y.R. Duan, Y. Dong, CXCR4-targeted ultrasound microbubbles for imaging and enhanced chemotherapy/immunotherapy in liver cancer, Acta Biomater. 197 (2025) 416–430, https://doi.org/10.1016/j.actbio.2025.03.018.

[18] J.A. Kopechek, A.R. Carson, C.F. McTiernan, X. Chen, B. Hasjim, L. Lavery, M. Sen, J.R. Grandis, F.S. Villanueva, Ultrasound targeted microbubble destruction-mediated delivery of a transcription factor decoy inhibits STAT3 signaling and tumor growth, Theranostics 5 (2015) 1378–1387, https://doi.org/10.7150/thno.12822.

[19] Y. Zhou, H. Gu, Y. Xu, F. Li, S. Kuang, Z. Wang, X. Zhou, H. Ma, P. Li, Y. Zheng, H. Ran, J. Jian, Y. Zhao, W. Song, Q. Wang, D. Wang, Targeted antiangiogenesis gene therapy using targeted cationic microbubbles conjugated with CD105 antibody compared with untargeted cationic and neutral microbubbles, Theranostics 5 (2015) 399–417, https://doi.org/10.7150/thno.10351.

[20] S. Kotopoulis, G. Dimcevski, O. Helge Gilja, D. Hoem, M. Postema, Treatment of human pancreatic cancer using combined ultrasound, microbubbles, and gemcitabine: a clinical case study, Med. Phys. 40 (2013) 1–9, https://doi.org/10.1118/1.4808149.

[21] G. Dimcevski, S. Kotopoulis, T. Bjånes, D. Hoem, J. Schjøt, B.T. Gjertsen, M. Biermann, A. Molven, H. Sorbye, E. McCormack, M. Postema, O.H. Gilja, A human clinical trial using ultrasound and microbubbles to enhance gemcitabine treatment of inoperable pancreatic cancer, J. Control. Release 243 (2016) 172–181, https://doi.org/10.1016/j.jconrel.2016.10.007.

[22] B. Zhou, Q. Lian, C. Jin, J. Lu, L. Xu, X. Gong, P. Zhou, Human clinical trial using diagnostic ultrasound and microbubbles to enhance neoadjuvant chemotherapy in HER2- negative breast cancer, Front. Oncol. 12 (2022) 1–11, https://doi.org/10.3389/fonc.2022.992774.

[23] A. Rix, M. Piepenbrock, B. Flege, S. von Stillfried, P. Koczera, T. Opacic, N. Simons, P. Boor, S. Thoröe-Boveleth, R. Deckers, J.N. May, T. Lammers, G. Schmitz, E. Stickeler, F. Kiessling, Effects of contrast-enhanced ultrasound treatment on neoadjuvant chemotherapy in breast cancer, Theranostics 11 (2021) 9557–9570, https://doi.org/10.7150/THNO.64767.

[24] M. Haram, R. Hansen, D. Bouget, O.F. Myhre, C. de, L. Davies, E. Hofsli, Treatment of liver metastases with focused ultrasound and microbubbles in patients with colorectal cancer receiving chemotherapy, Ultrasound Med. Biol. 49 (2023) 2081–2088, https://doi.org/10.1016/j.ultrasmedbio.2023.05.013.

[25] A. Bellary, A. Villarreal, R. Eslami, Q.J. Undseth, B. Lec, A.M. Defnet, N. Bagrodia, J.J. Kandel, M.A. Borden, S. Shaikh, R. Chopra, T.W. Laetsch, L.J. Delaney, C. M. Shaw, J.R. Eisenbrey, S.L. Hernandez, S.R. Sirsi, Perfusion-guided sonopermeation of neuroblastoma: a novel strategy for monitoring and predicting liposomal doxorubicin uptake in vivo, Theranostics 10 (2020) 8143–8161, https://doi.org/10.7150/thno.45903.

[26] S.M. Chowdhury, L. Abou-Elkacem, T. Lee, J. Dahl, A.M. Lutz, Ultrasound and microbubble mediated therapeutic delivery: underlying mechanisms and future outlook, J. Control. Release 326 (2020) 75–90, https://doi.org/10.1016/j.jconrel.2020.06.008.

[27] B. van Elburg, J. Deprez, M. van den Broek, S.C. De Smedt, M. Versluis, G. Lajoinie, I. Lentacker, T. Segers, Dependence of sonoporation efficiency on microbubble size: an in vitro monodisperse microbubble study, J. Control. Release 363 (2023) 747–755, https://doi.org/10.1016/j.jconrel.2023.09.047.

[28] M.A. Baig, Y. Du, Z. Zan, Z. Fan, Influence of cell shape on sonoporation efficiency in microbubble-facilitated delivery using micropatterned cell arrays, Sci. Rep. 14 (2024) 1–16, https://doi.org/10.1038/s41598-024-81410-1.

[29] Y. Yang, Q. Li, X. Guo, J. Tu, D. Zhang, Mechanisms underlying sonoporation: interaction between microbubbles and cells, Ultrason. Sonochem. 67 (2020) 105096, https://doi.org/10.1016/j.ultsonch.2020.105096.

[30] J. Blöck, H. Li, G. Collado-Lara, K. Kooiman, A. Rix, J. Chen, C. Hark, H. Radermacher, C. Porte, F. Kiessling, The Compression-Dominated ultrasound response of Poly(n-butyl cyanoacrylate) Hard-Shelled microbubbles induces significant sonoporation and sonopermeation effects in vitro, ACS Appl. Bio Mater. 8 (2025) 1240–1250, https://doi.org/10.1021/acsabm.4c01551.

[31] M. Moosavifar, R.A. Barmin, E. Rama, A. Rix, R.A. Gumerov, T. Lisson, C. Bastard, S. Rütten, N. Avraham-Radermacher, J. Koehler, M. Pohl, V. Kulkarni, J. Baier, S. Koletnik, R. Zhang, A. Dasgupta, A. Motta, M. Weiler, I.I. Potemkin, G. Schmitz, F. Kiessling, T. Lammers, R.M. Pallares, Polymeric microbubble shell engineering: microporosity as a key factor to enhance ultrasound imaging and drug delivery performance, 2404385, Adv. Sci. (2024) 1–13, https://doi.org/10.1002/advs.202404385.

[32] S. Fokong, A. Fragoso, A. Rix, A. Curaj, Z. Wu, W. Lederle, O. Iranzo, J. Gätjens, F. Kiessling, M. Palmowski, Ultrasound molecular imaging of E-Selectin in tumor vessels using poly n-butyl cyanoacrylate microbubbles covalently coupled to a short targeting peptide, Invest. Radio. 48 (2013) 843–850, https://doi.org/10.1097/RLI.0b013e31829d03ec.

[33] P. Koczera, L. Appold, Y. Shi, M. Liu, A. Dasgupta, V. Pathak, T. Ojha, S. Fokong, Z. Wu, M. van Zandvoort, O. Iranzo, A.J.C. Kuehne, A. Pich, F. Kiessling, T. Lammers, PBCA-based polymeric microbubbles for molecular imaging and drug delivery, J. Control. Release 259 (2017) 128–135, https://doi.org/10.1016/j.jconrel.2017.03.006.

[34] A. Rix, S. Fokong, S. Heringer, R. Pjontek, L. Kabelitz, B. Theek, M.A. Brockmann, M. Wiesmann, F. Kiessling, Molecular ultrasound imaging of αvβ3-integrin expression in carotid arteries of pigs after vessel injury, Invest. Radio. 51 (2016) 767–775, https://doi.org/10.1097/RLI.0000000000000282.

[35] A. Dasgupta, T. Sun, E. Rama, A. Motta, Y. Zhang, C. Power, D. Moeckel, S. M. Fletcher, M. Moosavifar, R. Barmin, C. Porte, E.M. Buhl, C. Bastard, R. M. Pallares, F. Kiessling, N. McDannold, S. Mitragotri, T. Lammers, Transferrin Receptor-Targeted nonspherical microbubbles for Blood–Brain barrier sonopermeation, Adv. Mater. 35 (2023) 1–11, https://doi.org/10.1002/adma.202308150.

[36] J.N. May, S.K. Golombek, M. Baues, A. Dasgupta, N. Drude, A. Rix, D. Rommel, S. Von Stillfried, L. Appold, R. Pola, M. Pechar, L. Van Bloois, G. Storm, A.J. C. Kuehne, F. Gremse, B. Theek, F. Kiessling, T. Lammers, Multimodal and multiscale optical imaging of nanomedicine delivery across the blood-brain barrier upon sonopermeation, Theranostics 10 (2020) 1948–1959, https://doi.org/10.7150/thno.41161.

[37] B. Theek, M. Baues, T. Ojha, D. Möckel, S.K. Veettil, J. Steitz, L. Van Bloois, G. Storm, F. Kiessling, T. Lammers, Sonoporation enhances liposome accumulation and penetration in tumors with low EPR, J. Control. Release 231 (2016) 77–85, https://doi.org/10.1016/j.jconrel.2016.02.021.

[38] Corning Incorporated Life Sciences, Collagen coating transwell ® inserts from corning protocol, 2009, pp. 0–1. ⟨www.corning.com/lifesciences⟩.

[39] J. Chen, B. Wang, Y. Wang, H. Radermacher, J. Qi, J. Momoh, T. Lammers, Y. Shi, A. Rix, F. Kiessling, mRNA sonotransfection of tumors with polymeric microbubbles: co-formulation versus co-administration, 2306139, Adv. Sci. (2024) 1–12, https://doi.org/10.1002/advs.202306139.

[40] C. Hark, J. Chen, J. Blöck, E.M. Buhl, H. Radermacher, R. Pola, M. Pechar, T. Etrych, Q. Peña, A. Rix, N.I. Drude, F. Kiessling, T. Lammers, J.N. May, RGD-coated polymeric microbubbles promote ultrasound-mediated drug delivery in an inflamed endothelium-pericyte co-culture model of the blood-brain barrier, Drug Deliv. Transl. Res. 14 (2024) 2629–2641, https://doi.org/10.1007/s13346-024-01561-6.

[41] N. Otsu, P.L. Smith, D.B. Reid, C. Environment, L. Palo, P. Alto, P.L. Smith, Otsu_1979_otsu_method, IEEE Trans. Syst. Man. Cybern. C. (1979) 62–66.

[42] B.A. Pulaski, S. Ostrand-Rosenberg, Mouse 4T1 breast tumor model, Curr. Protoc. Immunol. 39 (2000), https://doi.org/10.1002/0471142735.im2002s39.

[43] I. De Cock, E. Zagato, K. Braeckmans, Y. Luan, N. de Jong, S.C. De Smedt, I. Lentacker, Ultrasound and microbubble mediated drug delivery: acoustic pressure as determinant for uptake via membrane pores or endocytosis, J. Control. Release 197 (2015) 20–28, https://doi.org/10.1016/j.jconrel.2014.10.031.

[44] B. Helfield, X. Chen, S.C. Watkins, F.S. Villanueva, Transendothelial perforations and the sphere of influence of Single-Site sonoporation, Ultrasound Med. Biol. 46 (2020) 1686–1697, https://doi.org/10.1016/j.ultrasmedbio.2020.02.017.

[45] J.P. Ross, X. Cai, J.-F. Chiu, J. Yang, J. Wu, Optical and atomic force microscopic studies on sonoporation, J. Acoust. Soc. Am. 111 (2002) 1161–1164, https://doi.org/10.1121/1.1448340.

[46] N. Sheikov, N. McDannold, S. Sharma, K. Hynynen, Effect of focused ultrasound applied with an ultrasound contrast agent on the tight junctional integrity of the brain microvascular endothelium, Ultrasound Med. Biol. 34 (2008) 1093–1104, https://doi.org/10.1016/j.ultrasmedbio.2007.12.015.

[47] K. Kooiman, M. Emmer, M. Foppen-Harteveld, A. Van Wamel, N. De Jong, Increasing the endothelial layer permeability through ultrasound-activated microbubbles, IEEE Trans. Biomed. Eng. 57 (2010) 29–32, https://doi.org/10.1109/TBME.2009.2030335.

[48] L. Cucullo, P.O. Couraud, B. Weksler, I.A. Romero, M. Hossain, E. Rapp, D. Janigro, Immortalized human brain endothelial cells and flow-based vascular modeling: a marriage of convenience for rational neurovascular studies, J. Cereb. Blood Flow. Metab. 28 (2008) 312–328, https://doi.org/10.1038/sj.jcbfm.9600525.

[49] D. Kim, S. Eom, S.M. Park, H. Hong, D.S. Kim, A collagen gel-coated, aligned nanofiber membrane for enhanced endothelial barrier function, Sci. Rep. 9 (2019) 1–11, https://doi.org/10.1038/s41598-019-51560-8.
[50] R. Booth, H. Kim, Characterization of a microfluidic in vitro model of the blood-brain barrier (μBBB), Lab Chip 12 (2012) 1784–1792, https://doi.org/10.1039/c2lc40094d.
[51] L.M. Griep, F. Wolbers, B. De Wagenaar, P.M. Ter Braak, B.B. Weksler, I.A. Romero, P.O. Couraud, I. Vermes, A.D. Van Der Meer, A. Van Den Berg, BBB on CHIP: microfluidic platform to mechanically and biochemically modulate blood-brain barrier function, Biomed. Micro 15 (2013) 145–150, https://doi.org/10.1007/s10544-012-9699-7.
[52] P. Qin, Y. Lin, L. Jin, L. Du, A.C.H. Yu, Impact of microbubble-to-cell parameters on heterogeneous sonoporation at the single-cell level, 2015, IEEE Int. Ultrason. Symp. IUS 2015 (2015) 10–13, https://doi.org/10.1109/ULTSYM.2015.0292.
[53] C. Jud, S. Ahmed, L. Müller, C. Kinnear, D. Vanhecke, Y. Umehara, S. Frey, M. Liley, S. Angeloni, A. Petri-Fink, B. Rothen-Rutishauser, Ultrathin ceramic membranes as scaffolds for functional cell coculture models on a biomimetic scale, Biores. Open Access 4 (2015) 457–468, https://doi.org/10.1089/biores.2015.0037.
[54] O. Eikrem, S. Kotopoulis, M. Popa, M.M. Safont, K.O. Fossan, S. Leh, L. Landolt, J. Babickova, O.A. Gudbrandsen, O.H. Gilja, B. Riedel, J. Schjøtt, E. McCormack, H. P. Marti, Ultrasound and microbubbles enhance uptake of doxorubicin in murine kidneys, Pharmaceutics 13 (2021), https://doi.org/10.3390/pharmaceutics13122038.
[55] F.A. Duck, Acoustic properties of tissue at ultrasonic frequencies, Phys. Prop. Tissues (1990) 73–135, https://doi.org/10.1016/b978-0-12-222800-1.50008-5.
[56] T. Li, Y.N. Wang, T.D. Khokhlova, S. D'Andrea, F. Starr, H. Chen, J.S. McCune, L. J. Risler, A. Mashadi-Hossein, J.H. Hwang, Pulsed high-intensity focused ultrasound enhances delivery of doxorubicin in a preclinical model of pancreatic cancer, Cancer Res 75 (2015) 3738–3746, https://doi.org/10.1158/0008-5472.CAN-15-0296.
[57] P.T. Yemane, A.K.O. Åslund, S. Snipstad, A. Bjørkøy, K. Grendstad, S. Berg, Y. Mørch, S.H. Torp, R. Hansen, C. de, L. Davies, Effect of ultrasound on the vasculature and extravasation of nanoscale particles imaged in real time, Ultrasound Med. Biol. 45 (2019) 3028–3041, https://doi.org/10.1016/j.ultrasmedbio.2019.07.683.
[58] M. Olsman, V. Sereti, K. Andreassen, S. Snipstad, A. van Wamel, R. Eliasen, S. Berg, A.J. Urquhart, T.L. Andresen, C. de, L. Davies, Ultrasound-mediated delivery enhances therapeutic efficacy of MMP sensitive liposomes, J. Control. Release 325 (2020) 121–134, https://doi.org/10.1016/j.jconrel.2020.06.024.
[59] E. Sulheim, I. Hanson, S. Snipstad, K. Vikedal, Y. Mørch, Y. Boucher, C. de, L. Davies, Sonopermeation with Nanoparticle-Stabilized microbubbles reduces solid stress and improves nanomedicine delivery to tumors, Adv. Ther. 4 (2021), https://doi.org/10.1002/adtp.202100147.
[60] C.Y. Lin, H.C. Tseng, H.R. Shiu, M.F. Wu, C.Y. Chou, W.L. Lin, Ultrasound sonication with microbubbles disrupts blood vessels and enhances tumor treatments of anticancer nanodrug, Int. J. Nanomed. 7 (2012) 2143–2152, https://doi.org/10.2147/IJN.S29514.
[61] C.T. Chin, B.I. Raju, T. Shevchenko, A.L. Klibanov, Control and reversal of tumor growth by ultrasound activated microbubbles. Proc, IEEE Ultrason. Symp, 2009, pp. 77–80, https://doi.org/10.1109/ULTSYM.2009.5441604.
[62] X. Hu, A. Kheirolomoom, L.M. Mahakian, J.R. Beegle, D.E. Kruse, K.S. Lam, K. W. Ferrara, Insonation of targeted microbubbles produces regions of reduced blood flow within tumor vasculature, Invest. Radio. 47 (2012) 398–405, https://doi.org/10.1097/RLI.0b013e31824bd237.
[63] V. Frenkel, A. Etherington, M. Greene, J. Quijano, J. Xie, F. Hunter, S. Dromi, K.C. P. Li, Delivery of liposomal doxorubicin (Doxil) in a breast cancer tumor model: investigation of potential enhancement by pulsed-high intensity focused ultrasound exposure, Acad. Radio. 13 (2006) 469–479, https://doi.org/10.1016/j.acra.2005.08.024.
[64] C.Y. Lin, J.R. Li, H.C. Tseng, M.F. Wu, W.L. Lin, Enhancement of focused ultrasound with microbubbles on the treatments of anticancer nanodrug in mouse tumors, Nanomed. Nanotechnol. Biol. Med. 8 (2012) 900–907, https://doi.org/10.1016/j.nano.2011.10.005.
[65] M. Cagel, M.A. Moretton, E. Bernabeu, M. Zubillaga, E. Lagomarsino, S. Vanzulli, M.B. Nicoud, V.A. Medina, M.J. Salgueiro, D.A. Chiappetta, Antitumor efficacy and cardiotoxic effect of doxorubicin-loaded mixed micelles in 4T1 murine breast cancer model. Comparative studies using Doxil® and free doxorubicin, J. Drug Deliv. Sci. Technol. 56 (2020) 101506, https://doi.org/10.1016/j.jddst.2020.101506.
[66] O. Tezcan, A.S. Elshafei, K. Benderski, E. Rama, M. Wagner, D. Moeckel, R. Pola, M. Pechar, T. Etrych, S. von Stillfried, F. Kiessling, R. Weiskirchen, S. Meurer, T. Lammers, Effect of cellular and microenvironmental multidrug resistance on Tumor-Targeted drug delivery in Triple-Negative breast cancer, J. Control. Release 354 (2023) 784–793, https://doi.org/10.1016/j.jconrel.2022.12.056.
[67] M.A. Miller, Y.R. Zheng, S. Gadde, C. Pfirschke, H. Zope, C. Engblom, R.H. Kohler, Y. Iwamoto, K.S. Yang, B. Askevold, N. Kolishetti, M. Pittet, S.J. Lippard, O. C. Farokhzad, R. Weissleder, Tumour-associated macrophages act as a slow-release reservoir of nano-therapeutic Pt(IV) pro-drug, Nat. Commun. 6 (2015), https://doi.org/10.1038/ncomms9692.
[68] S. Fokong, M. Siepmann, Z. Liu, G. Schmitz, F. Kiessling, J. Gätjens, Advanced characterization and refinement of poly N-Butyl cyanoacrylate microbubbles for ultrasound imaging, Ultrasound Med. Biol. 37 (2011) 1622–1634, https://doi.org/10.1016/j.ultrasmedbio.2011.07.001.
[69] J. Qi, J. Chen, S. Von Stillfried, P. Kozcera, Y. Shi, A. Rix, F. Kiessling, Molecular ultrasound imaging with clinically translatable cRGD-Coated microbubbles to assess αvβ3-Integrin expression in inflammatory bowel disease, Invest. Radio. 00 (2024) 1–7, https://doi.org/10.1097/RLI.0000000000001143.
[70] Y. Barenholz, Doxil® - the first FDA-approved nano-drug: lessons learned, J. Control. Release 160 (2012) 117–134, https://doi.org/10.1016/j.jconrel.2012.03.020.
[71] J.J. Choi, W. Wang, Y.-S. Shougang, B. Tung, I.I.I. Morrison, E.E. Konofagou, Molecules of various pharmacologically-relevant sizes can cross the ultrasound-induced blood-brain barrier opening in vivo, Ultrasound Med. Biol. 36 (2010) 58–67, https://doi.org/10.1016/j.ultrasmedbio.2009.08.006.
[72] T. Ojha, G.J.L. Schaefer, R. Mihyar, V. Pathak, J. Ehling, E. Rama, F. De Lorenzi, A. S. Elshafei, D. Moeckel, S. Elsafy, B. Theek, M. Wagner, P. Ceccarini, L. Consolino, M. Weiler, F. Peisker, T. Caspers, Q. Pena, R. Barmin, F. Gremse, R. Pola, M. Pechar, T. Etrych, S. Meurer, R. Weiskirchen, R. Kramann, F. Kiessling, G. Storm, J. Metselaar, T. Lammers, Desmoplastic tumor priming using clinical-stage corticosteroid liposomes, Cell Biomater. 1 (2025) 1–15, https://doi.org/10.1016/j.celbio.2025.100051.

Glossary

FBS: Fetal bovine serum
FITC: Fluorescein isothiocyanate
fUS: Focused ultrasound
HUVEC: Human umbilical vein endothelial cells
MBs: Microbubbles
MMPs: Matrix metalloproteinases
NaCl: Sodium chloride
P/S: Penicillin and streptomycin
PBCA: Poly(butyl cyanoacrylate)
PNP: Peak negative pressure
RPMI: Roswell Park Memorial Institute
TEER: Transepithelial/ endothelial electrical resistance
US: Ultrasound
VEGF: Vascular endothelial growth factor
WGA: Wheat germ agglutinin